Virologica Sinica 39 (2024) 587–599

Contents lists available at ScienceDirect

Virologica Sinica

journal homepage: www.keaipublishing.com/en/journals/virologica-sinica
www.virosin.org

Research Article

Pseudorabies virus VHS protein abrogates interferon responses by blocking NF-κB and IRF3 nuclear translocation

Zhenfang Yan [a], Jiayu Yue [a], Yaxin Zhang [a], Zhengyang Hou [a], Dianyu Li [a], Yanmei Yang [b], Xiangrong Li [a,c,d], Adi Idris [e], Huixia Li [a], Shasha Li [b], Jingying Xie [a,b,*], Ruofei Feng [a,c,d,*]

[a] Key Laboratory of Biotechnology and Bioengineering of State Ethnic Biomedical Research Center, Northwest Minzu University, Lanzhou, 730030, China
[b] College of Life Science and Engineering, Northwest Minzu University, Lanzhou, 730030, China
[c] Gansu Tech Innovation Center of Animal Cell, Biomedical Research Center, Northwest Minzu University, Lanzhou, 730030, China
[d] Engineering Research Center of Key Technology and Industrialization of Cell-based Vaccine, Ministry of Education, Biomedical Research Center, Northwest Minzu University, Lanzhou, 730030, China
[e] Centre for Immunology and Infection Control, School of Biomedical Sciences, Queensland University of Technology, Kelvin Grove, Queensland, 4702, Australia

ARTICLE INFO

Keywords:
Pseudorabies virus (PRV)
UL41
IRF3
Interferon
cGAS-STING

ABSTRACT

Herpesviruses antagonize host antiviral responses through a myriad of molecular strategies culminating in the death of the host cells. Pseudorabies virus (PRV) is a significant veterinary pathogen in pigs, causing neurological sequalae that ultimately lead to the animal's demise. PRV is known to trigger apoptotic cell death during the late stages of infection. The virion host shutdown protein (VHS) encoded by UL41 plays a crucial role in the PRV infection process. In this study, we demonstrate that UL41 inhibits PRV-induced activation of inflammatory cytokine and negatively regulates the cGAS-STING-mediated antiviral activity by targeting IRF3, thereby inhibiting the translocation and phosphorylation of IRF3. Notably, mutating the conserved amino acid sites (E192, D194, and D195) in the RNase domain of UL41 or knocking down UL41 inhibits the immune evasion of PRV, suggesting that UL41 may play a crucial role in PRV's evasion of the host immune response during infection. These results enhance our understanding of how PRV structural proteins assist the virus in evading the host immune response.

1. Introduction

PRV is an alpha herpesvirus that shares many common characteristics of *Herpesviridae*, including a wide range of host targets, potent latent infection, and neurotrophic properties. Cortical proteins encoded by this virus family play key roles in virus assembly and release (Pomeranz et al., 2005; Drolet et al., 2010), regulation of viral or host gene transcription, and immune evasion (Radtke et al., 2010; Sandbaumhüter et al., 2013). Pseudorabies, also known as Aujeszky's disease (AD) or mad itch, is an acute febrile disease caused by PRV, leading to encephalomyelitis and respiratory disease in livestock, particularly prevalent during the spring and winter. PRV is a pansophilic virus, capable of infecting most vertebrates, including its natural host, pigs (Meier et al., 2015). PRV infection in pigs causes serious disease and has negative impacts on the global pig livestock economy (Sehl and Teifke, 2020). Worryingly, cases of PRV causing respiratory and neurological infections in humans have been reported, suggesting that PRV can cross over to human hosts (Wang et al., 2020; Tan et al., 2021). Therefore, understanding the molecular pathogenesis of PRV and the mechanism of evading the host immune response is essential.

As the primary defense against infectious agents, innate immunity can initiate innate immune signaling pathways and lead to the production of type I interferons (IFN-I) (Deng et al., 2022). Recent investigations have highlighted the improtance of the cGAMP synthase-stimulator of interferon genes (cGAS-STING) signaling axis in the host's response to herpesvirus infection (Jin et al., 2023). However, herpesviruses have devolved mechanisms to counteract the cGAS-STING pathway, aiming to suppress or evade innate immune responses elicited by constant immune pressure exerted by the host (Ge and Ding, 2022). The nuclear factor NF-kappa B (NF-κB) signaling pathway plays a critical role in antiviral defense, as it enhances the antiviral capability of host cells by regulating the transcription of multiple interferon genes, including interferon α, β, and γ (Ersing et al., 2013). NF-κB is a critical component of innate immune signaling cascades and activates the expression of

* Corresponding authors.
E-mail addresses: fengruofei@xbmu.edu.cn (R. Feng), xjy_1314@126.com (J. Xie).

https://doi.org/10.1016/j.virs.2024.05.009
Received 5 January 2024; Accepted 23 May 2024
Available online 30 May 2024

pro-inflammatory cytokine genes. It is activated by heterodimerization and mainly consists of p65 and p50 subunits (Perkins, 2007). Studies have demonstrated that herpes simplex virus (HSV-1) can both activate and repress the NF-κB pathway, primarily to promote the survival of infected cells or evade from antiviral defenses. HSV-1 encoding protein UL36 inhibits the degradation of inhibitor of kappa B alpha (IκBα) by de-ubiquitination, maintaining the inactive state of NF-κB, and prevents the activation of NF-κB (Ye et al., 2017).

VHS is a protein encoded by the *UL41* gene (unique long region 41), which has similar endonuclease activity and substrate properties to RNase A (Pasieka et al., 2008). It has been demonstrated to disrupt the antigen presentation (Samady et al., 2003; He et al., 2020). UL41 is highly conserved across herpesviruses. However, numerous studies exploring the molecular mechanisms of PRV immune evasion rely on research conducted on HSV-1 homologs. HSV UL41 can specifically interact with the translation initiation factor complex, splices mRNA at the translation initiation site, and then induce a rapid shutdown of host protein synthesis (Page and Read, 2010). HSV UL41 also selectively degrades target mRNA during the early stages of infection (Geiss et al., 2000; Dauber et al., 2016). At the late stage of infection, HSV UL41 binds to other viral proteins, such as VP16, and dampens their normal regulatory function. HSV UL41 also blocks the expression of various interferon stimulated genes (ISGs). The VHS homology protein, encoded by open reading frame (ORF) 17 in varicella-zoster virus, induces a delayed shutoff of cellular RNA translation (Desloges et al., 2005). However, the VHS homology protein encoded by ORF19 of equid herpesvirus type 1, cannot degrade mRNAs or induce the shutoff of cellular and viral protein synthesis (Stokol and Soboll Hussey, 2019). The VHS homologous protein encoded by PRV can induce host mRNA degradation and cleave the internal ribosome entry site (IRES) sequence containing RNA (Liu et al., 2016). Additionally, the VHS homologous protein of duck plague virus (DPV) affects pol II mRNA degradation, protein synthesis shutoff, and viral replication and spread (He et al., 2021). Furthermore, the VHS homologous protein of bovine herpesvirus (BoHV-1) degrades the 5′ cap and 3′ untranslated region adenylate-uridylate-rich element areas of signal transducer of activation 1 (STAT1) in the antiviral pathway (Ma et al., 2019).

Since the *Herpesviridae* UL41 protein plays an important role in immune evasion during the late stages of infection, this study aims to elucidate the role and mechanism of PRV UL41 in innate immune responses. As a double-stranded DNA (dsDNA) virus, we were also interested in whether PRV interacts with the innate immune cytoplasmic DNA sensing adaptors cGAS-STING and further activates NF-κB signaling pathways. Our findings will provide new insights into the complex molecular interplay between the host innate immune machinery and PRV, contributing to a better understanding of PRV pathogenesis.

2. Materials and methods

2.1. Cells and viruses

Porcine kidney (PK-15) and human embryonic kidney (HEK-293) cells were obtained from ATCC and cultured in DMEM supplemented with 10% new bovine serum (NBS) at 37 °C in a 5% CO_2 incubator. PRV-JL was propagated in baby hamster kindney-21 (BHK-21) cells, and the supernatants of infected cells were clarified and stored at −80 °C.

2.2. Antibodies and reagents

HRP-conjugated goat anti-rabbit IgG (1:5000, D110058) and HRP-conjugated goat anti-mouse IgG (1:5000, D110087) were purchased from Sangon Biotech (Shanghai, China). NF-κB p65 rabbit polyclonal antibody (1:1000, 10745-1-AP), GAPDH mouse monoclonal antibody (1:2000, 60004-1-Ig), Myc tag mouse monoclonal antibody (1:1000, 60003-2-Ig), NF-κB1 rabbit polyclonal antibody (1:1000, 14220-1-AP), IκB Alpha Polyclonal antibody (1:500, 10268-1-AP), TAK1 rabbit polyclonal antibody (1:1000, 12330-2-AP), Anti-Flag tag rabbit polyclonal antibody (1:1000, 80010-1-RR), Anti-Flag tag Mouse Monoclonal antibody (1:1000, 66008-4-Ig), and VDAC1/Porin polyclonal antibody (1:1000, 55259-1-AP) were purchased from Proteintech (Wuhan, China). Phospho-IκBα (Ser32/36) rabbit polyclonal antibody (1:300, AF5851) from Beyotime (Shanghai, China). HA-tagged polyclonal antibody (1:1000, 51064-2-AP) and IRF3 polyclonal antibody (1:1000, 11312-1-AP) were purchased from Proteintech (Wuhan, China); STING (D2P2F) Rabbit mAb (1:1000, 13647S), phospho-IRF3 (Ser386) (E7J8G) XP® Rabbit mAb antibody (1:1000, 37829S) were purchased from Cell Signaling Technology. Anti-HIST3H3 polyclonal antibody (1:1000, K106623P) were purchased from Solarbio (Beijing, China). β-actin mouse monoclonal antibody (1:5000, AA128) were purchased from Beyotime Biotechnology (Shanghai, China).

TransStart® Top Green qPCR SuperMix (+Dye II) was purchased from Transgen (Beijing, China). Cell membrane/cytoplasm/nuclear membrane protein step extraction kit (BB-31042) was purchased from BestBio (Shanghai, China). Lipofectamine 3000 was purchased from Invitrogen. Chemical reagents RNase inhibitor (Thermo Fisher, Waltham, MA, USA), MG132 (7.5 μM, Beyotime, Nantong, China), chloroquine (50 μmol/L, CQ) (tlrl-chq, InvivoGen, San Diego, CA, USA), Z-VAD-FMK (20 μmol/L, Beyotime) Ac-DEVD-CHO (20 μmol/L, Beyotime), Z-IETD-FMK (20 μmol/L, MedChemExpress), Z-LEHD-FMK TFA (20 μmol/L, MedChemExpress), TNF-α (20 μmol/L, InvivoGen), poly(dA:dT) (2 μg, InvivoGen), 2′3′-cGAMP (2 μg, InvivoGen) and poly(I:C) (2 μg, InvivoGen) were purchased from indicated manufacturers.

2.3. Western blotting

The Western blotting was conducted as described previously (Han et al., 2021). In brief, cells were harvested and whole-cell extracts were prepared with lysis buffer RIPA (Solarbio, Beijing, China). Cell extracts were subjected to 10% or 15% SDS-PAGE, and the separated proteins were transferred to PVDF membranes (Millipore, Berlington, MA, USA). GAPDH or β-actin served as loading control. The proteins were detected using ECL Blotting Substrate (Bio-Rad, Hercules, CA, USA).

2.4. Real-time qPCR for determination of relative gene expression

mRNA transcription levels for NF-κB-dependent genes such as IFN-β, ISGs (ISG15 and MX1), TNF-α, IL-6 and IL-8 were determined by relative quantitative PCR (RT-qPCR). Cellular RNA was isolated and reverse-transcribed to cDNA. Methods were performed as previously described (Han et al., 2021). The mean mRNA fold changes relative to the control were calculated using the $2^{-\Delta\Delta CT}$ method. The primers are listed in Supplementary Table S1.

2.5. Transfection

In PK-15 cells, the plasmid transfections were conducted with Lipofectamine 3000 (Invitrogen, Waltham, MA, USA). All experiments were performed according to the manufacturer's instructions. Cells were then infected with PRV for 24 h at a multiplicity of infection (MOI) of 0.001 (except for the cases mentioned in the figure legends) to test the effect of UL41 on PRV replication. In co-transfection experiments, UL41 and reporter gene constructs were transfected in a 1:1 mass ratio.

2.6. RNA interference

Predesigned siRNA oligomers were obtained from the Sigma-Aldrich based on the porcine Tollip, NDP52 and p62 mRNA sequences published in GenBank. Specific siTollip, siNDP52 and sip62 with non-targeting control siNC were transfected for 24 h. Knockdown efficiency was verified by immunoblotting. The siRNA primers are listed in Supplementary Table S2.

2.7. $TCID_{50}$ assay

BHK-21 cells were cultured in 96-well plates and infected with 10-fold diluted PRV. The 50% tissue culture infective dose ($TCID_{50}$) was calculated using the method of Reed and Muench.

2.8. Flow cytometry

After the cells were digested into single cells with 0.25% trypsin, cells were washed thrice with PBS and stained with the annexin V-APC apoptosis detection kit. An excitation wavelength of 633 nm and a maximum emission wavelength of 660 nm were used to measure cell fluorescence using a Beckman flow cytometer. Analysis was carried out using FlowJo software (v10.8.1; Tree Star, Inc., Ashland, OR).

2.9. Co-immunoprecipitation (Co-IP)

The Co-IP was conducted as described previously (Han et al., 2021). HEK-293 cells were collected with lysis buffer supplemented with phosphatase inhibitor cocktail. The cell lysate was then incubated with the indicated antibody or control IgG at 4 °C overnight. Subsequently, 20 μL of Protein G agarose slurry (Beyotime, Nantong, China) was added to each lysate. After incubation for 4 h at 4 °C, the lysates were centrifuged at 2500×*g* for 5 min. The beads were collected and washed 5 times with ice-cold PBS. The precipitates were mixed with SDS buffer and boiled for 5 min at 95 °C. After centrifugation at 6000×*g* or 1 min, the supernatant was collected and used for Western blot analysis.

2.10. Confocal microscopy

PK-15 cells were seeded in 12-well plates (5×10^5 cells/well). After 24 h, cells were fixed in 4% paraformaldehyde for 10 min at 25 °C and then gently washed three times with PBS. Cells were blocked and permeabilized with 0.5% Triton X-100, 5% skimmed milk at 4 °C overnight. Finally, cells were incubated with the indicated primary and secondary antibodies and DAPI. Images were acquired with a Zeiss microscope (LSM 900) and 63 × objectives to visualize stained cells. Fluorescence intensity profiles of the indicated proteins were measured using the Zen Blue program.

2.11. Nuclear and cytoplasmic protein extraction

Nuclear and cytoplasmic proteins were extracted using the Cell membrane/cytoplasm/nuclear membrane protein step extraction kit (BB-31042) (BestBio, Shanghai, China)) according to the manufacturer's instruction. The respective protein extracts were analyzed by standard immunoblotting procedures.

2.12. Mitochondria and cytoplasmic extraction

Mitochondrial Isolation Reagent (Beyotime, C3601) were added to PK-15 cells, and left on ice for 15 min before homogenizing for about 10–30 strokes and centrifuged at 600 g at 4 °C for 10 min. Supernatant were then further centrifuge at 11,000×*g* at 4 °C for 10 min. The precipitates were analyzed by standard immunoblotting procedures.

2.13. Statistical analysis

All experiments were performed at least three times. Data are presented as the mean ± standard deviation. The statistical analyses were performed by GraphPad Prism 5. Statistical analysis was used a *t*-test or one-way ANOVA with a Tukey post-hoc test. A P-value < 0.05 was considered statistically significant.

3. Results

3.1. UL41 suppresses PRV-triggered proinflammatory and IFN responses

We wondered whether PRV UL41 could antagonize pro-inflammatory and IFN-I antiviral responses like other herpesviruses (Pheasant et al., 2018). A significant reduction in cytokine and ISG responses was observed in PRV-infected PK-15 cells overexpressing UL41 (Fig. 1A). As PRV is a dsDNA virus, we hypothesized that UL41 could block the IFN-I responses in the host cytosolic DNA sensing cGAS-STING machinery. When cGAS detects viral DNA, it undergoes a conformational change, converting GTP and ATP to cGAMP. This process activates the STING receptor, resulting in the downstream phosphorylation of TANK-binding kinase 1 (TBK1) and IkappaB kinase (IKK) adaptor proteins to further initiate the nuclear translocation of IRF3 and NF-κB. This culminates in the induction of IFN-I and pro-inflammatory cytokines. Increasing exogenous UL41 expression significantly inhibited pro-inflammatory and IFN-I responses in cells stimulated with two distinct cGAS-STING agonists, poly(dA:dT) (Figs. 1B) and 2′3′-cGAMP (Fig. 1C). These results indicate that UL41 may be exerting its antagonistic function within the cGAS-STING pathway.

3.2. UL41 inhibits type I IFN responses via the blockade and degradation of IRF3

We reasoned that UL41 might antagonize IFN-I responses by inhibiting the function of IRF3, a crucial component of innate antiviral immunity that viruses usually exploit to suppress antiviral responses. Importantly, IRF3 can also inhibit the activity of NF-κB, the pro-inflammatory transcription factor, to dampen inflammatory cytokine responses (Popli et al., 2022). We observed that co-expression of UL41 with cGAS-STING signaling components resulted in apparent inhibition of *IFN-β* gene expression activated by these components (Fig. 2A). Moreover, the attenuation of cGAS-STING agonist-triggered IFN response by UL41 coincides with the observed reduction in levels of both unphosphorylated and phosphorylated forms of IRF3 (Fig. 2B and C). Importantly, we confirm that UL41 can directly interact with IRF3 through biochemical assay (Fig. 2D and E) and confocal microscopy (Fig. 2F). IRF3 is an important adapter in the cGAS-STING signaling pathway. The phosphorylation of IRF3 and its subsequent translocation into the nucleus are essential for the downstream transcriptional activation of antiviral genes (Ming et al., 2022). Nucleo-cytoplasmic separation experiments revealed that UL41 can block IRF3 expression in the nucleus, consistent with the notion that IRF3 nuclear translocation is impeded, thus blocking transcriptional activation of IFN-I (Fig. 2G).

3.3. UL41 degrades IRF3 via the tollip-mediated autophagy pathway

Considering these observations, we postulated that UL41 could directly promote the degradation of IRF3. To verify this, we treated PK-15 cells overexpressing IRF3 and UL41 with proteasome (MG132), autophagy (CQ), and the broad-spectrum caspase (Z-VAD-FMK) inhibitors. Immunoblotting analysis revealed that UL41 is indeed inhibiting IRF3 protein expression through the autophagy pathway (Fig. 3A). Viruses that achieve natural immune escape through the autophagy pathway require the recruitment of specific selective autophagy receptors to link viral proteins to target proteins. Indeed, endogenous IRF3 is known to interact with autophagy proteins, NDP52 and p62 (Wu et al., 2021; Xie et al., 2022). Co-immunoprecipitation (Co-IP) experiments showed that UL41 interacted with several other selective autophagy receptors (Fig. 3B), in particular Tollip (Fig. 3C). Specifically, we observed a significant increase of LC3-II levels in UL41-overexpressing PK-15 cells compared to untreated cells, indicating that UL41 promotes activation of the autophagic pathway. We also found that the knockdown of Tollip slowed the activation of the autophagic pathway (Fig. 3D). To further

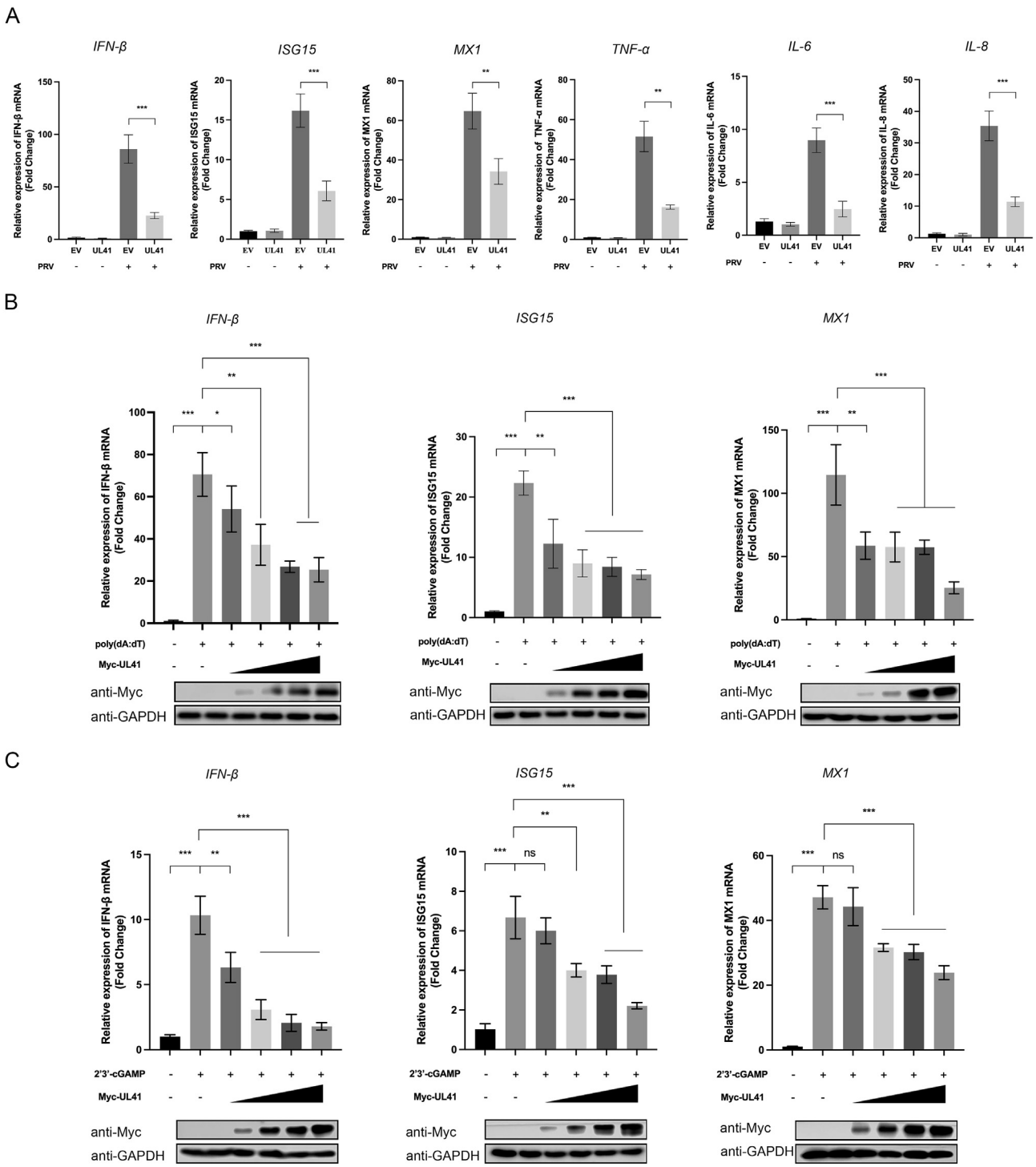

Fig. 1. UL41 suppresses the mRNA levels of IFN-β, TNF-α, IL-6, IL-8 and ISGs. **A** PK-15 cells were transfected with pCMV-Myc empty vector or Myc tagged UL41 expression plasmid for 24 h. Then cells were either uninfected or infected with PRV (MOI = 0.001) for 18 h and total RNA was extracted for RT-qPCR of the indicated genes. **B, C** Myc-tagged UL41 (200 ng, 500 ng, 800 ng and 1 μg) plasmid was transfected into PK-15 cells for 24 h, and then either left untreated or treated with poly(dA:dT) (**B**) or 2′3′-cGAMP (**C**) (2 mg/mL) for 12 h. The mRNA expression levels of indicated genes were determined by RT-qPCR. The expression of UL41 was detected with Myc specific antibody. GAPDH serves as a loading control. Data from at least three independent experiments are presented as the mean ± standard deviation. $^{*}P < 0.05$, $^{**}P < 0.01$, $^{***}P < 0.001$; ns, not significant. Western blot images are the representatives of three independent experiments.

dissect mechanism on how UL41 drives the degradation of IRF3 by autophagy, UL41 was co-expressed with IRF3 and individual Myc-tagged autophagy proteins before performing immunoblotting analysis. We observed that the inhibition of IRF3 by UL41 was more pronounced when Tollip is overexpressed (Fig. 3E). Furthermore, siRNA knockdown of Tollip alleviated the inhibitory effect of UL41 on IRF3 (Fig. 3F). Regardless of the knockdown of NDP52 or p62, overexpression of UL41 is unable to effectively counteract the degradation of IRF3. These results suggest that UL41 promote IRF3 degradation by recruiting the selective autophagy receptor Tollip.

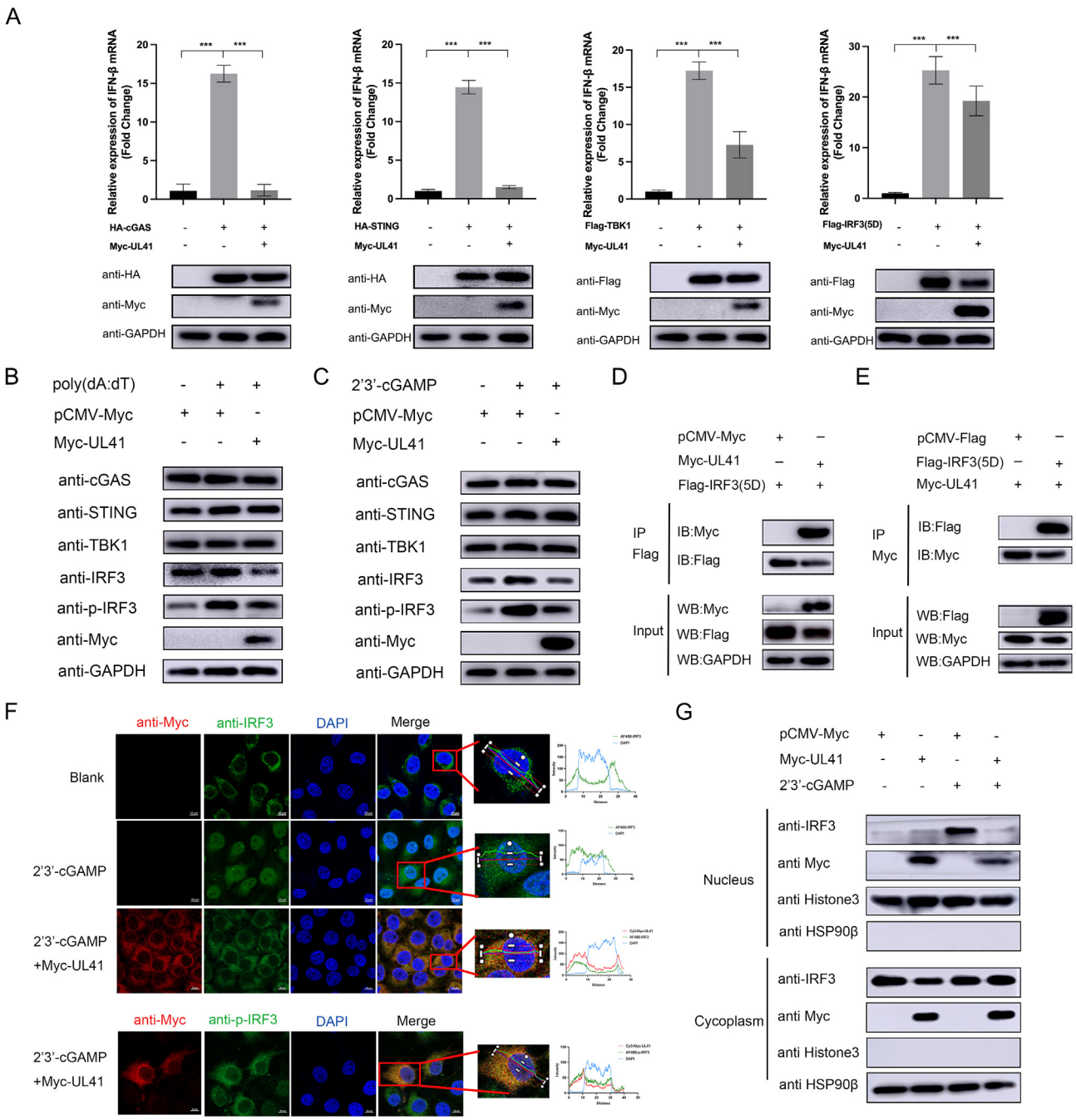

Fig. 2. UL41 degrades IRF3 and inhibites the cGAS-STING-mediated phosphorylation of IRF3. **A** PK-15 cells were cultured overnight in 6-well plates. The indicated plasmids (HA-cGAS, HA-STING, Flag-TBK1, and Flag-IRF3(5D) (500 ng) were co-transfected into PK-15 cells with Myc-tagged UL41 (1 μg) for 24 h. The expression of cGAS, STING, TBK1, IRF3, and UL41 proteins were detected using antibodies against HA, Myc and Flag. GAPDH serves as a loading control. The transcription level of IFN-β was detected by RT-qPCR. **B, C** Myc-tagged UL41 plasmid was transfected into PK-15 cells for 24 h, and then either left untreated or treated with poly(dA:dT) (2 mg/mL) (**B**) or 2′3′-cGAMP (2 mg/mL) (**C**) for 12 h. The expression of cGAS, STING, TBK1, IRF3, phosphorylation IRF3 and UL41 proteins were detected using indicated antibodies. GAPDH serves as a loading control. **D, E** HEK-293 cells were co-transfected with Flag-tagged IRF3 (5D) (1 μg) and Myc-tagged UL41 (1 μg) expression plasmid for 24 h. Cells were processed for IP with anti-Flag or anti-Myc beads. Inputs and precipitated proteins were probed with antibodies against Flag-tag, Myc-tag, and GAPDH. **F** Myc-tagged UL41 (1 μg) plasmid was transfected into PK-15 cells for 24 h and either left untreated or treated with 2′3′-cGAMP (2 mg/mL). Cells were stained with anti-Myc (red), anti-IRF3 (green) and anti-p-IRF3 (green) subjected to analysis by confocal microscopy. Nuclei were stained with DAPI (blue). Scale bars, 10 μm. **G** Myc-tagged UL41 plasmid (1 μg) was transfected into PK-15 cells for 24 h, and then either left untreated or treated with 2′3′-cGAMP (2 g/mL). Then, cytoplasmic and nuclear proteins were extracted and subjected to Western blot analysis. Expression of IRF3 and Myc-tagged UL41 was detected with specific antibodies. Histone 3 was used as a nuclear protein marker. HSP90β served as a cytoplasm marker. + represents for transfected, and – represents for untransfected. Data from at least three independent experiments are presented as the mean ± standard deviation. ***$P < 0.001$. Western blot, fluorescence images, and Co-IP results are representatives of three independent experiments.

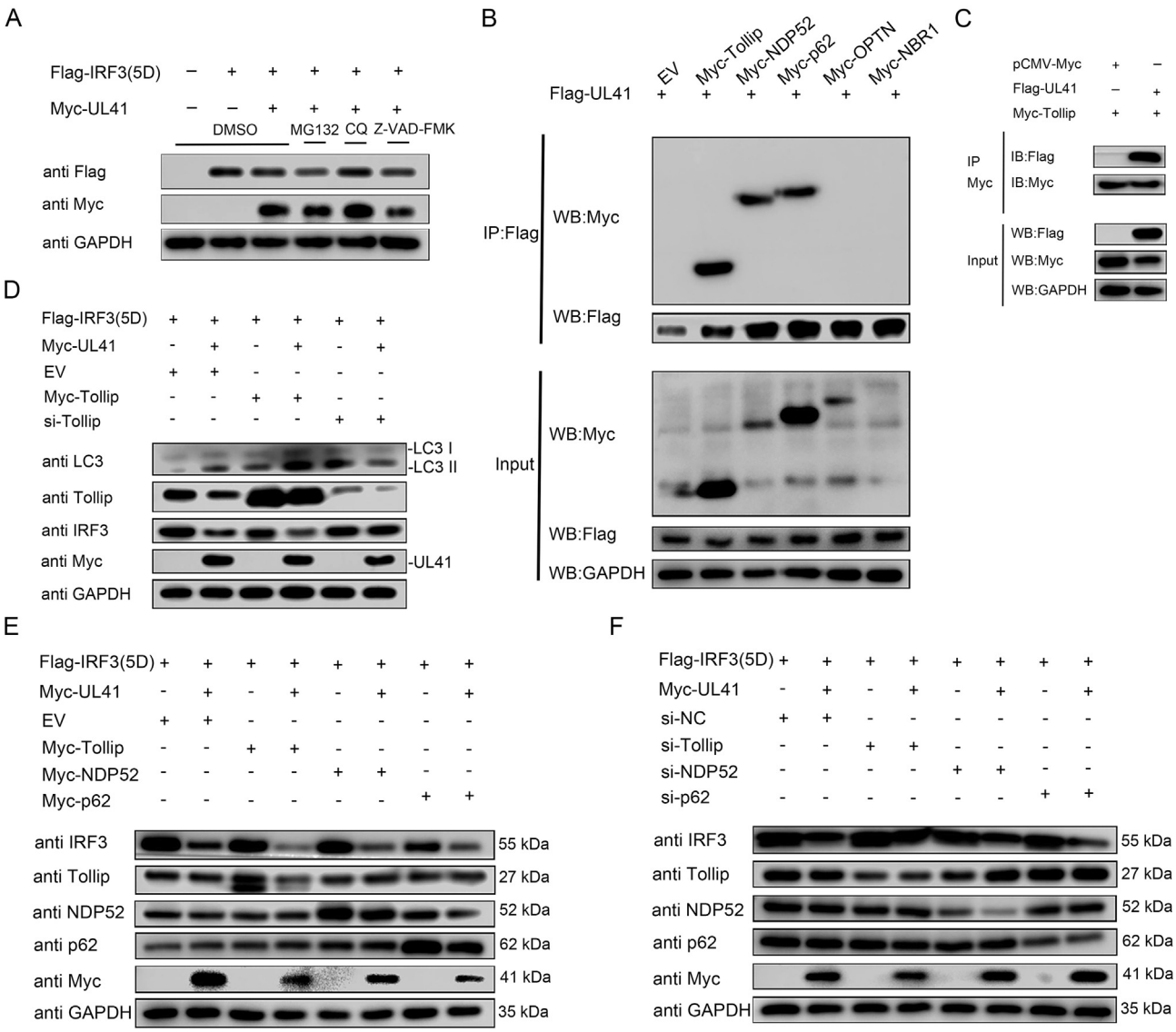

Fig. 3. UL41 recruits Tollip to promote IRF3 autophagic degradation. **A** PK-15 cells were co-transfected with Flag tagged IRF3(5D) (1 μg), Myc-tagged UL41 (1 μg) or pCMV-Myc empty vector (EV) (1 μg) for 24 h, then cells were treated with proteasomal inhibitor MG132 (7.5 μmol/L), lysosome inhibitor CQ (50 μmol/L) or caspase inhibitor Z-VAD-FMK (20 μmol/L) for 12 h. DMSO treated cells served as vehicle control. Cells were collected and immunoblotted for Flag-tagged IRF3 and Myc-tagged UL41. GAPDH served as loading control. **B, C** HEK-293 cells were co-transfected with Myc-tagged autophagy receptor expression plasmids (Tollip, NDP52, p62, OPTN and NBR1) (1 μg) and Flag-tagged UL41 (1 μg) expression plasmids for 24 h. Cells were processed for IP with anti-Flag or anti-Myc beads. Inputs and precipitated proteins were probed with antibodies against Flag-tag, Myc-tag, and GAPDH. **D** PK-15 cells were co-transfected with Tollip or siTollip, Flag-tagged IRF3(5D) and Myc-tagged UL41 for 24 h. LC3, IRF3, Tollip and Myc tagged UL41 were assessed by immunoblot analysis. GAPDH served as a loading control. **E** HEK-293 cells were co-transfected with Myc-tagged autophagy receptor expression plasmids (Tollip, NDP52, p62) (1 μg) or Flag-tagged IRF3(5D) (1 μg) and Myc-tagged UL41 (1 μg) for 24 h. IRF3, Tollip, NDP52, p62, Myc tagged UL41 and GAPDH were assessed by immunoblot analysis. **F** HEK-293 cells were transfected with siNC, siTollip, siNDP52, sip62 or Flag-tagged IRF3(5D) (1 μg) and Myc-tagged UL41 (1 μg) as indicated for 24 h. IRF3, Tollip, NDP52, p62, Myc tagged UL41 and GAPDH were assessed by immunoblot analysis. Western blot and Co-IP results are representatives of three independent experiments.

3.4. UL41 dampens TNF-α mediated NF-κB activation via the intrinsic apoptotic pathway

TNF-α primarily initiates proinflammatory cytokine responses via the NF-κB signaling pathway (Karin et al., 2002). Earlier, we observed that UL41 inhibits PRV-induced activation of pro-inflammatory cytokines IL-6 and IL-8. We then assessed the impact of UL41 on exogenous TNF-α-mediated induction of *IL-6* and *IL-8* gene expression. In two distinct cell lines (HEK-293 and PK-15 cells), UL41 exhibited inhibitory activity in TNF-α-mediated IL-6 and IL-8 expression (Fig. 4A). We hypothesized that the observed cytokine dampening effect of UL41 occurs at the level of the NF-κB signaling cascade. Overexpression of UL41 resulted in a significant reduction in the level of the NF-κB p50 subunit, regardless of whether cells were unexposed (Fig. 4B) or exposed to TNF-α (Fig. 4C). This suggests that p50 is a target site of UL41.

To elucidate the mechanism by which UL41 triggers p50 degradation, we assessed the contribution of the proteasomal, autophagic and apoptotic machineries. Using chemical inhibitors against these pathways, we observed that UL41 degrades TNF-α-activated p50 through both autophagy and apoptotic pathways (Fig. 5A). Co-IP analysis further validates the importance of caspase proteins in UL41-mediated targeting of p50 (Fig. 5B). Notably, confocal microscopy reveals that TNF-α facilitates the nuclear translocation of p50, while UL41 effectively blocks its nuclear entry (Fig. 5C). Collectively, our findings demonstrate that PRV UL41 can dampen TNF-α mediated NF-κB activation via the intrinsic apoptotic pathway.

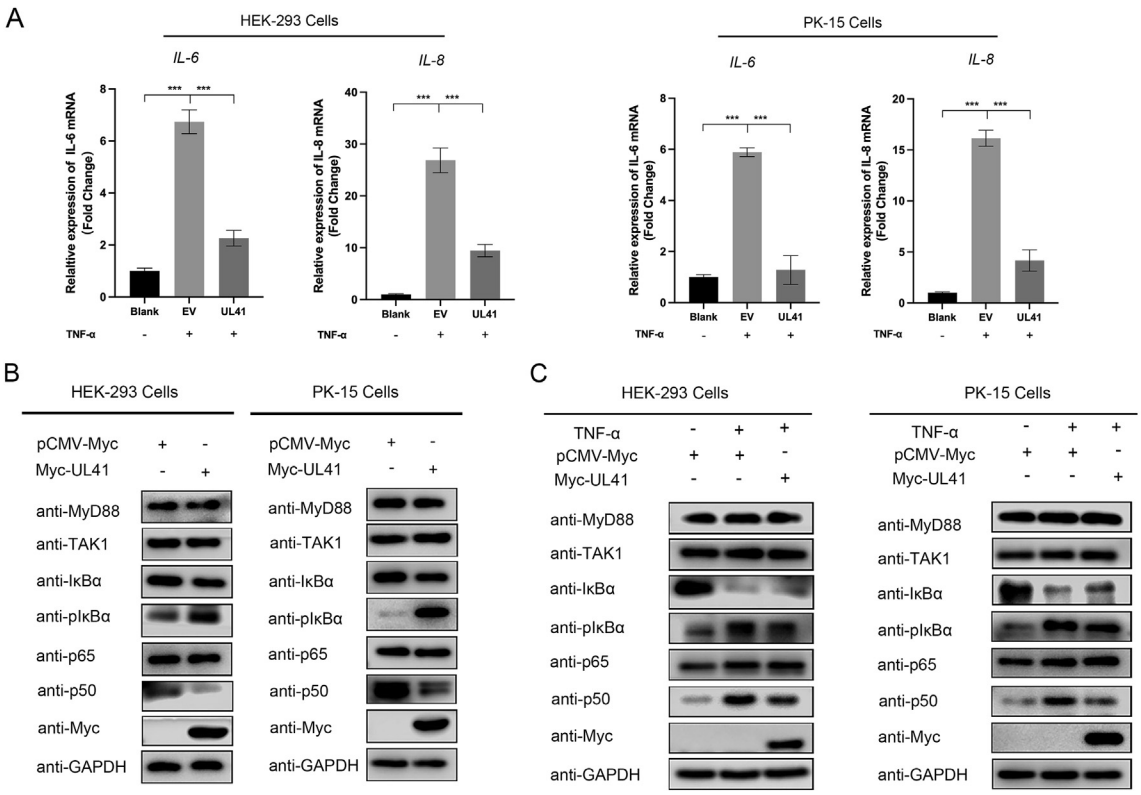

Fig. 4. UL41 Dampens TNF-α-mediated NF-κB activation. **A** HEK-293 and PK-15 cells were transfected with pCMV-Myc empty vector (1 μg) or Myc tagged UL41 (1 μg) expression plasmid. At 24 h post-transfection, the cells were treated with TNF-α (10 ng/mL) for 12 h. Total cellular RNA was extracted and transcription level of IL-6 and IL-8 was analyzed by RT-qPCR. **B** HEK-293 and PK-15 cells were transfected with pCMV-Myc empty vector (1 μg) or Myc tagged UL41 (1 μg) expression plasmid. At 24 h post-transfection, the expression of MyD88, TAK1, IκBα, p-IκBα, p65, p50 and Myc tagged UL41 were detected by western blotting. GAPDH serves as a loading control. **C** HEK-293 and PK-15 cells were transfected with pCMV-Myc empty vector (1 μg) or Myc tagged UL41 (1 μg) expression plasmid. At 24 h post-transfection, the cells were treated with TNF-α (10 ng/mL) for 12 h. The expression of MyD88, TAK1, IκBα, p-IκBα, p65, p50 and Myc tagged UL41 were detected by Western blotting. GAPDH serves as a loading control. Data from at least three independent experiments are presented as the mean ± standard deviation. ***$P < 0.001$. Western blot results are representatives of three independent experiments.

3.5. UL41 promotes apoptosis in PK-15 cells

Pseudorabies is known to cause severe neurological damage in piglets as evidenced by the propensity for PRV to damage nerve cells. However, the mechanism by which PRV induces cell death remains unknown. PRV induces significant cytotoxicity in PK-15 cells, leading to apoptotic cell death within 20-h period (Fig. 6A and B). A marked increase in PRV UL41 gene expression was observed concurrently with massive apoptosis (Fig. 6C). Those results demonstrate that UL41 plays a role in inducing apoptosis in PK-15 cells (Fig. 6D). Mitochondria, along with apoptotic mediators, such as B-cell lymphoma 2 (Bcl-2) and Cytochrome *c* (Cyto-C), play an important role in regulating the endogenous apoptotic pathway. During viral infection, Bcl-2 is down-regulated thus promoting the release of Cyto-C from mitochondria, thereby facilitating the apoptotic process (Nomura et al., 1999). UL41 downregulated PRV-mediated Bcl-2 expression and conversely upregulated Cyto-C gene expression (Fig. 6E and F). At the protein level, PRV infection inhibits Bcl-2 expression, and this inhibition is further potentiated by UL41 (Fig. 6G). Subsequently, UL41 overexpression increases the levels of Cyto-C in the cytosol, with the converse being observed in the mitochondria (Fig. 6H). This suggests the activation of mitochondrial-dependent apoptotic programming. The NF-κB signaling pathway is known to play a role in blocking apoptosis (Kim et al., 2002). We previously observed a positive temporal correlation between apoptosis induction in PRV-infected cells and UL41 expression. We aimed to further explore whether UL41 promotes apoptosis by inhibiting NF-κB function, and whether apoptotic effector factors play a role in the PRV-mediated apoptotic cell death. By using various apoptotic caspase protein-specific inhibitors (caspase 3 inhibitor (Ac-DEVD-CHO), caspase 8 inhibitor (Z-IETD-FMK) and caspase 9 inhibitor (Z-LEHD-FMK TFA) in the presence of TNF-α, we observed that UL41-mediated inhibition of p50 could occur via caspases 3 and 9, which are important mediators in the intrinsic mitochondrial apoptotic pathway (Fig. 6I). Overall, our findings demonstrate that UL41 is intricately interlaced within the mitochondrial-mediated apoptotic machinery.

3.6. UL41 RNase domain is indispensable for its immune evasive function and PRV survival

Comparing the amino acid sequences of UL41 from PRV strains with those encoded by other α-herpesviruses, the results revealed a conserved region within the RNase domain region (Fig. 7A). To determine whether mutating these identified residues in UL41 (UL41-M) can disrupt its function, we replaced residues E192, D194 and D195 of PRV UL41 with alanine (A) as these residues are essential for the RNase activity of PRV UL41 (Zhang et al., 2017). Indeed, UL41-M has lost the ability to inhibit both TNF-α-mediated cytokine activation (Fig. 7B and C) and the expression of NF-κB subunit p50 (Fig. 7D). Importantly, UL41-M has lost its inhibitory effect on downregulating IRF3 and p-IRF3 (Fig. 7E). Co-IP analysis confirms that UL41-M does not directly interact with IRF3 (Fig. 7F), and consistent results were obtained through confocal microscopy (Fig. 7G). Given the immune evasive function of UL41, we surmised that UL41 enhances the survival and replication of PRV in host cells. As predicted, UL41, not UL41-M, significantly enhanced PRV

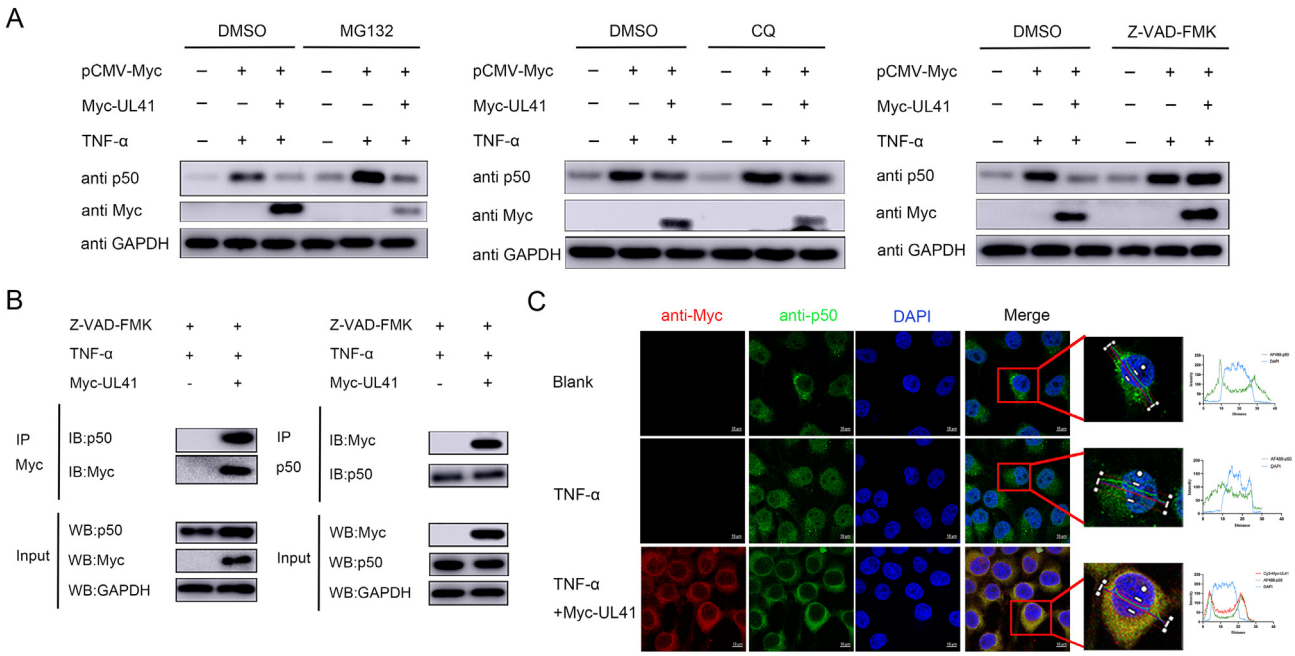

Fig. 5. UL41 targets p50 to inhibit NF-κB signaling. **A** PK-15 cells were transfected with Myc tagged UL41 (1 μg) or pCMV-Myc empty vector (EV) (1 μg) for 12 h following by stimulating with TNF-α (10 ng/mL) for another 12 h. Cells were treated with proteasomal inhibitor MG132 (7.5 μmol/L), lysosome inhibitor CQ (50 μmol/L) or caspase inhibitor Z-VAD-FMK (50 μmol/L) for 12 h. DMSO treated cells served as vehicle control. Then, cells were collected and immunoblotted for p50 and Myc-tagged UL41. GAPDH served as loading control. **B** HEK-293 cells were transfected with Myc-tagged UL41 (1 μg) expression plasmid for 12 h following by stimulating with TNF-α (10 ng/mL) for another 12 h. Cells were treated with Z-VAD-FMK (50 μmol/L) for 12 h, and then processed for IP with anti-Myc or anti-p50 beads. Inputs and precipitated proteins were probed with antibodies against Myc-tag, p50, and GAPDH. **C** PK-15 cells were cotransfected with Myc-tagged UL41 (1 μg) expression plasmid for 24 h. Then, the cells were treated with TNF-α (10 ng/mL) for another 12 h. Cells were stained with anti-Myc (red) and anti-p50 (green) subjected to analysis by confocal microscopy. Nuclei were stained with DAPI (blue). Scale bars, 10 μm. Western blot, fluorescence images, and Co-IP results are representatives of three independent experiments.

replication and proliferation (Fig. 7H). Overall, we demonstrate that the RNase domain of UL41 is indispensable for its immune evasive function and PRV survival.

3.7. Knockdown of UL41 restores antiviral responses during a PRV infection

To test our hypothesis that PRV can block this antiviral response, a known TLR stimulator, poly(I:C), was transfected into PK-15 cells before challenging with PRV. As expected, poly(I:C)-mediated IFN-β and IL-6 induction was significantly reduced upon PRV challenge (Fig. 8A). Importantly, knockdown of UL41 restored the PRV-mediated degradation of endogenous p-IRF3 and NF-kB subunits, p50 and p65 (Fig. 8B). Overall, we show that loss of UL41 restores antiviral responses during a PRV infection.

4. Discussion

The host-pathogen interplay is a dynamic process, with many viruses evolving mechanisms to coexist with their hosts and establish long-term infections. PRV has developed complex innate immune evasion strategies (Wang et al., 2022; Jiang et al., 2022). In this study, we found that UL41 interacts with and degrades IRF3 via the autophagy pathway by recruiting the selective autophagy receptor Tollip, leading to the inhibition of IRF3 phosphorylation to suppress IFN-I response. We also observed that UL41 targets p50 to inhibit the activation of the NF-κB pathway, thereby inhibiting the activation of inflammatory cytokine. Furthermore, we demonstrated that UL41 indirectly inhibits the expression of Bcl-2, leading to the release of Cyto-C from mitochondria to the cytoplasm expression and the activation of the apoptotic pathway (Fig. 9).

In addition to activating antiviral response via IRF3, host cells can also trigger other antiviral signaling pathways through transcription factors, such as NF-κB, IRF1, and IRF7, to induce the transcription of pro-inflammatory genes that inhibit viral invasion. There is a crosstalk between IRF3 and NF-κB, whereby TLRs can simultaneously activate IRF3 and NF-κB phosphorylation and undergo nucleus translocation (Czerkies et al., 2018). Activated IRF3 dimerization is also able to form a complex with NF-κB and enter the nucleus to initiate IFN transcription. Previous reports have found that IRF3 can interact with subunits of NF-κB, and that these crosstalk effects during an antiviral state allow for faster activation of antiviral transcription factors (Popli et al., 2022). Triggering NF-κB activation during viral infection is a double-edged sword. On one hand, NF-κB activation prevents apoptosis and prolongs the survival time of infected cells, thus allowing sufficient time for replication. On the other hand, NF-κB plays a key role in triggering innate and adaptive immune and inflammatory responses, thereby limiting viral replication (Ghosh et al., 1998). Indeed, successful viral replication requires balanced NF-κB activation to evade the host immune response.

Autophagy is a highly conserved homeostatic process in eukaryotic cells, responsible for decomposing and recycling dysfunctional cellular components (Choi et al., 2018). Previous reports have suggested a link between PRV replication and autophagy. Sun et al. discovered that PRV can induce autophagy in the early stage of infection. However, the US3 protein can decrease autophagy levels by activating the AKT/mTOR pathway, thereby inhibiting PRV replication (Sun et al., 2017). It was found that alpha-herpesvirus UL21 induces cGAS degradation via TOLLIP-mediated autophagy, which negatively modulates innate immunity and promotes viral replication (Ma et al., 2023). Recent studies have shown that autophagy is a selective degradation system. Substrates such as damaged organelles or aggregated proteins are delivered to the autophagosome through cargo receptors (e.g., SQSTM1/p62, NBR1,

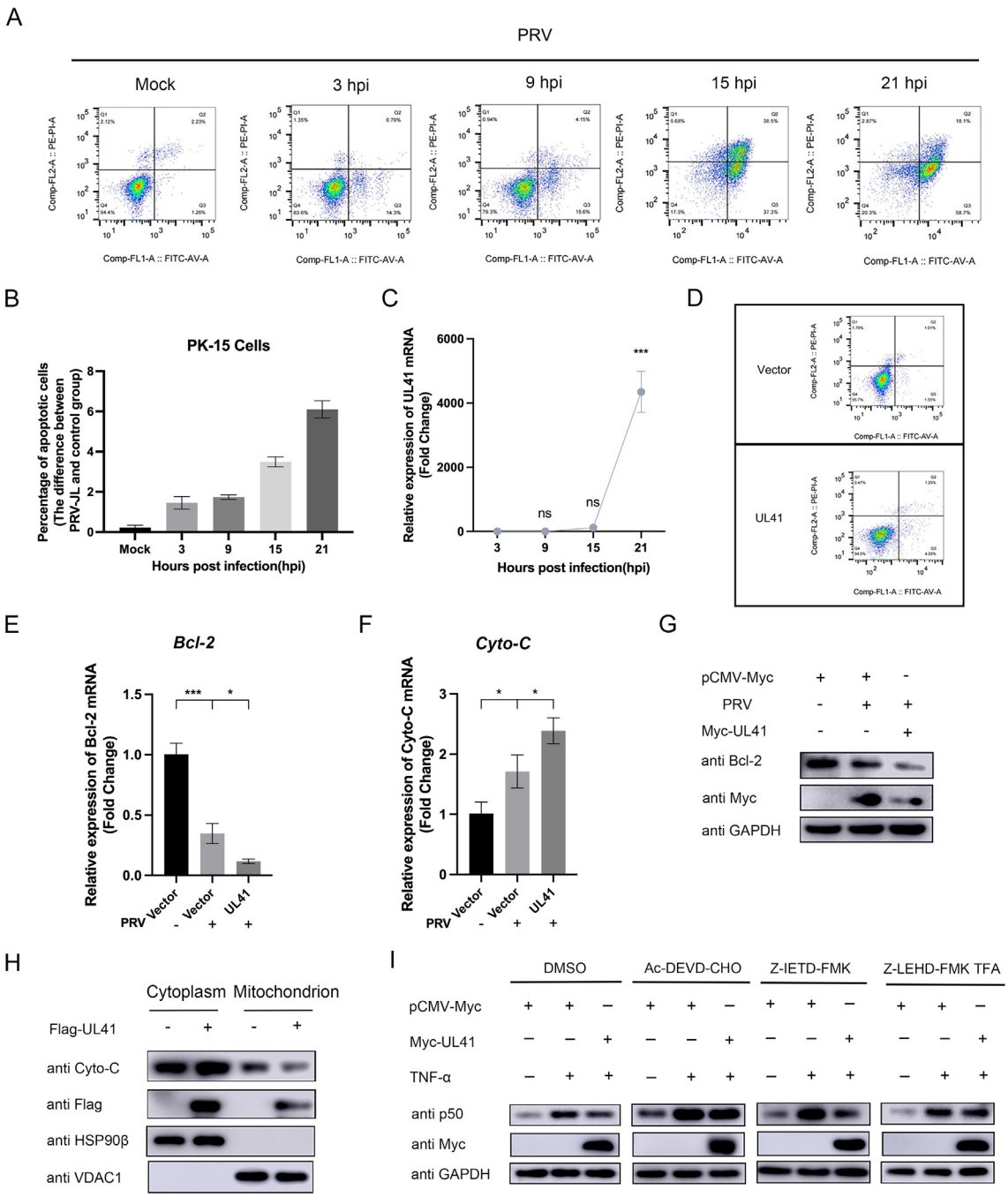

Fig. 6. UL41 promotes apoptosis in PK-15 cells. **A** PK-15 cells were infected with PRV (MOI = 1). Flow cytometry was used to determine apoptotic events by annexin V (AV-FITC) and propidium iodide (PI-PE) staining in PK-15 cells induced by PRV at 0, 3, 9, 15 and 21 h after infection. **B** Flow cytometry was used to detect apoptosis of PK-15 induced by PRV at 0, 3, 9, 15 and 21 h after infection. **C** PK-15 cells were infected with PRV (MOI = 1) for 0 h, 3 h, 8 h, 15 h and 21 h. The mRNA levels of PRV UL41 were assessed by RT-qPCR. **D** PK-15 cells were transfected with Myc tagged UL41 (1 μg) or pCMV-Myc empty vector (1 μg) for 24 h. Flow cytometry was used to determine apoptotic events by annexin V (AV-FITC) and propidium iodide (PI-PE) staining. **E, F** PK-15 cells were transfected with pCMV-Myc empty vector (1 μg) or Myc-tagged UL41 (1 μg) expression plasmid. At 24 h post-transfection, cells were uninfected or infected with PRV (MOI = 1) for 9 h and total RNA was extracted and the mRNA levels of *Bcl-2* and *Cyto-C* were assessed by RT-qPCR. **G** PK-15 cells were transfected with pCMV-Myc empty vector (1 μg) or Myc-tagged UL41 (1 μg) expression plasmid. At 24 h post-transfection, cells were uninfected or infected with PRV (MOI = 1) for 9 h. The protein expression level of Bcl-2 was detected by Western blot. GAPDH serves as a loading control. **H** PK-15 cells were transfected with pCMV-Flag empty vector (1 μg) or Flag-tagged UL41 (1 μg) expression plasmid for 24 h. Then, cytoplasmic and mitochondria proteins were extracted and subjected to Western blot analysis. Expression of Cyto-C and Flag-tagged UL41 was detected with specific antibodies. VDAC1 was used as a mitochondria protein marker. HSP90β served as a cytoplasm marker. **I** PK-15 cells were transfected with Myc tagged UL41 (1 μg) or pCMV-Myc empty vector (EV) (1 μg) for 12 h following by stimulating with TNF-α (10 ng/mL) for another 12 h. Cells were treated with Caspase3 inhibitor Ac-DEVD-CHO (20 nmol/L), Caspase8 inhibitor Z-IETD-FMK (20 nmol/L) or caspase9 inhibitor Z-LEHD-FMK TFA (20 nmol/L) for 12 h. DMSO treated cells served as vehicle control. Then, cells were collected and immunoblotted for p50 and Myc-tagged UL41. GAPDH served as a loading control. Data from at least three independent experiments are presented as the mean ± standard deviation. $^{*}P < 0.05$, $^{***}P < 0.001$; ns, not significant. Western blot results are representatives of three independent experiments.

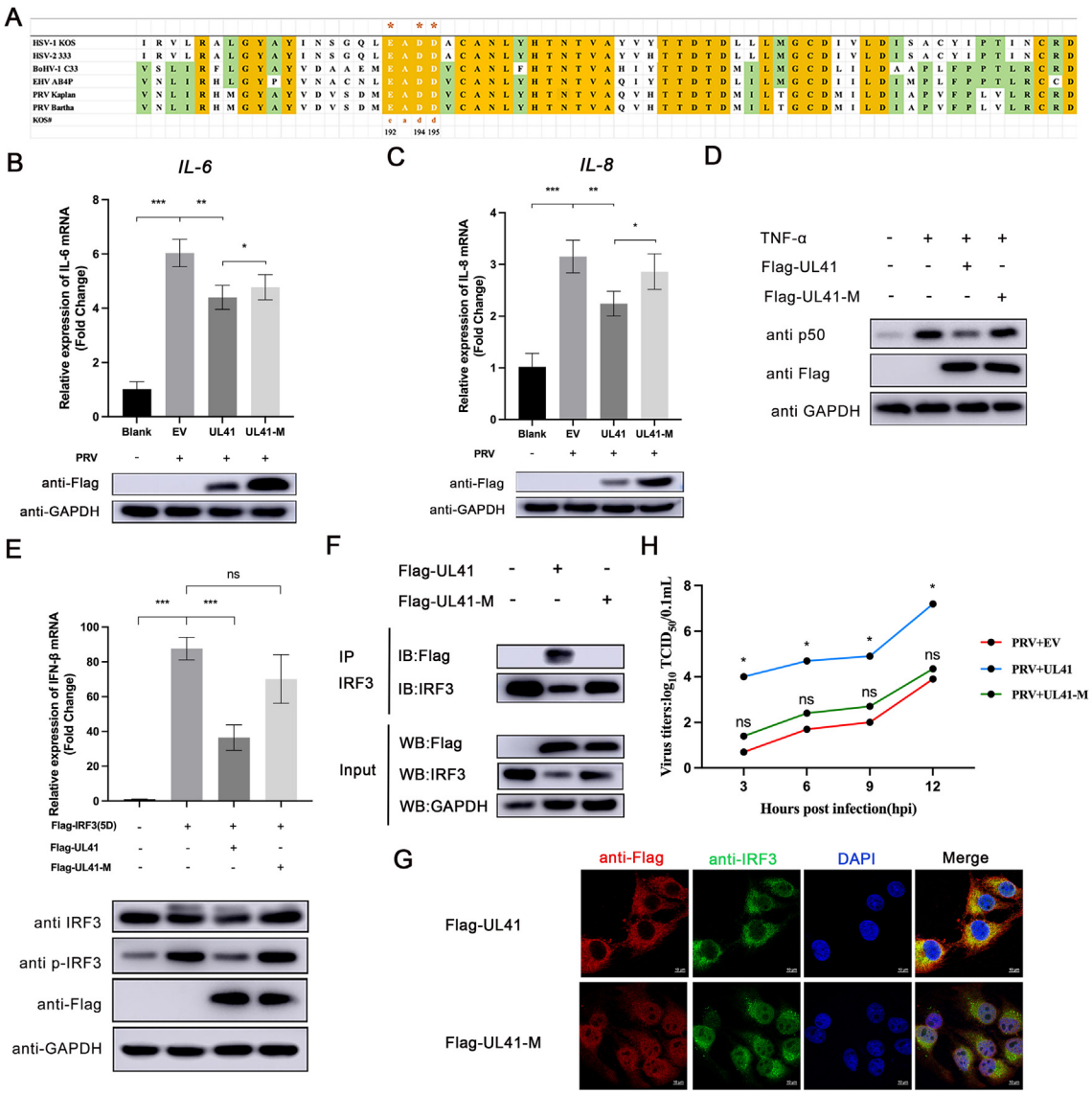

Fig. 7. E192, D194, and D195 sites of UL41 are critical for natural immune evasion. **A** Comparison of the amino acid sequences of the PRV UL41 protein and its homologs in alpha herpesviruses. **B, C** PK-15 cells were transfected with Flag-tagged-UL41-M (500 ng, 1 μg) expression plasmid. At 24 h post transfection, the cells were treated with TNF-α (10 ng/mL) for 12 h, and total cellular RNA was extracted. The fold change in gene expression of IL-6 or IL-8 was determined by RT-qPCR. The protein expression level of UL41-M was detected with Flag tag antibody. GAPDH serves as a loading control. **D** PK-15 cells were transfected with pCMV-Myc empty vector (1 μg) or Flag-tagged-UL41 (1 μg) and Flag-tagged-UL41-Mutant (1 μg) expression plasmid. At 24 h post transfection, the cells were treated with TNF-α (10 ng/mL) for 12 h. The expression of p50 was detected with specific antibody. UL41 and UL41-M expression were detected with Flag tag antibody. GAPDH serves as a loading control. **E** PK-15 cells were cultured overnight in 6-well plates. Flag-IRF3(5D) (1 μg) were co-transfected into cells with the indicated doses of Flag-tagged UL41 (1 μg) or Flag-tagged UL41-Mutant (1 μg) expression plasmid for 24 h. Cells were collected for IFN-β mRNA detection by RT-qPCR. IRF3, p-IRF3, Flag tagged UL41 and UL41-M were detected with indicated antibodies. GAPDH serves as a loading control. **F** HEK-293 cells were transfected with Flag-tagged UL41 (1 μg) or Flag-tagged UL41-M (1 μg) expression plasmids for 24 h. Cells were processed for IP with anti-IRF3 beads. Inputs and precipitated proteins were probed with antibodies against Flag-tag, IRF3, and GAPDH. **G** PK-15 cells were transfected with Flag-tagged UL41 (1 μg) or Flag-tagged UL41-M (1 μg) expression plasmids for 24 h. Cells were stained with anti-Flag (red) and anti-IRF3 (green) subjected to analysis by confocal microscopy. Nuclei were stained with DAPI (blue). Scale bars, 10 μm. **H** Exogenous expression of UL41 enhances PRV replication *in vitro*. PK-15 cells were transfected with 1 μg Flag tagged UL41 and Flag tagged UL41-M plasmid for 24 h. Then, cells were infected with PRV (MOI = 1) for 3 h, 6 h, 9 h and 12 h. $TCID_{50}$ assay was performed for viral titer detection. Data from at least three independent experiments are presented as the mean ± standard deviation. $^{*}P < 0.05$, $^{**}P < 0.01$, $^{***}P < 0.001$; ns, not significant. Western blot, fluorescence images, and Co-IP results are representatives of three independent experiments.

OPTN, CALCOCO2/NDP52, BNIP3L/Nix, and TOLLIP), and then degraded by lysosomes (Novak et al., 2010). There is increasing evidence suggesting that autophagy plays a crucial role in regulating immune responses. PRV UL41 is a viral ribonucleic acid endonuclease that facilitates the complex escape function of viruses during infection of host cells (Liu et al., 2015). We found that PRV UL41 significantly downregulated IRF3 expression and inhibited IRF3 phosphorylation and translocation into the nucleus (Figs. 1 and 2). Furthermore, UL41 inhibited IFN-β activation and repressed ISG activation by recruiting the selective autophagy receptor Tollip, which directly interacted with host IRF3. Indeed, UL41-mediated autophagic degradation via Tollip is essential to aid PRV escape (Fig. 3). Interestingly, we observed that UL41 interacted with p50, a subunit of NF-κB, and significantly down-regulated TNF-α-induced p50 expression. Although we initially hypothesized that UL41 inhibited the

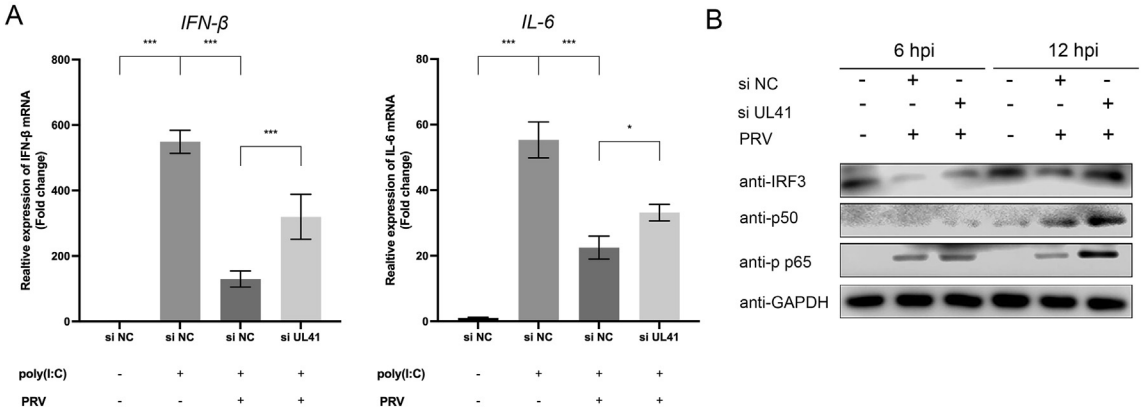

Fig. 8. Knockdown of UL41 promotes IFN-I pathway and NF-κB signaling activation. **A** PK-15 Cells were cultured overnight in 6-well plates, and si-UL41 and si-NC (non-targeting control) were transfected for 12 h. Then the cells were stimulated without or with poly(I:C) for 12 h, and uninfected or infected with PRV for 12 h. Cells were collected and total RNA were extracted for IFN-β and IL-6 mRNA detection by RT-qPCR. **B** PK-15 Cells were cultured overnight in 6-well plates, and si-UL41 and si-NC (nontargeting control) were transfected for 24 h. Subsequently, cells were infected without or with PRV (MOI = 1) for 6 h or 12 h. IRF3, p50 and p65 phosphorylation levels were examined using western blotting assay. GAPDH serves a loading control. Data from at least three independent experiments are presented as the mean ± standard deviation. $^{*}P < 0.05$, $^{***}P < 0.001$; ns, not significant. Western blot results are representatives of three independent experiments.

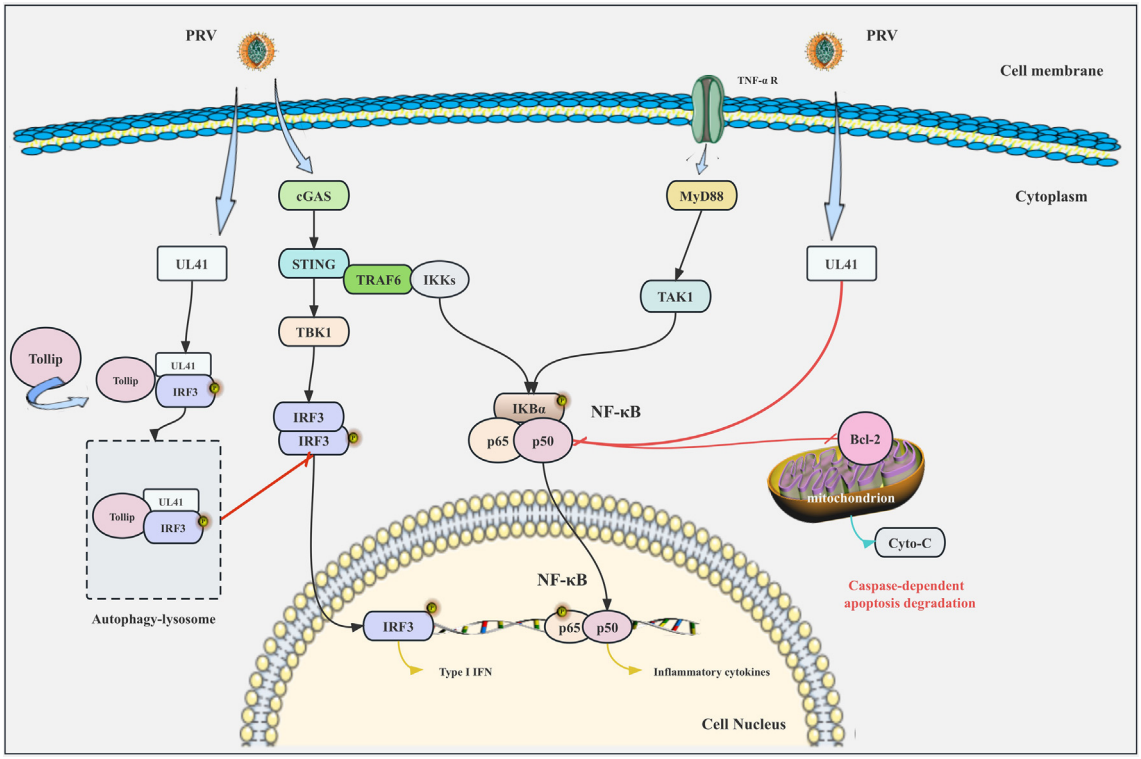

Fig. 9. Schematic representation of PRV UL41 targeting IRF3 to inhibit IFN-I activity. UL41 interacts with and degrades IRF3 via the autophagy pathway by inducing the selective autophagy receptor Tollip, followed by the inhibition of IRF3 phosphorylation to suppress the IFN-I response. UL41 targets p50 to inhibit the activation of the NF-κB pathway, which then inhibits IL-6 and IL-8 transcription. UL41 promotes the activation of the apoptotic pathway through the inhibition of Bcl-2, which in turn promotes the release of Cyto-C from mitochondria to the cytoplasm.

transcriptional levels of IL-6 and IL-8 by targeting p50, we found that UL41 degraded p50 via the intrinsic mitochondrial-apoptotic pathway (Figs. 4 and 5).

Bcl-2 can inhibit apoptosis by regulating genes that encode proteins necessary for programmed cell death by interfering with peroxidative damage. It can form a complex with p50 in the nucleus, leading to blocked gene expression in the nucleus (Hour et al., 2000; Bardel et al., 2016). To the best of our knowledge, there have been no reports of viral proteins promoting apoptosis by inhibiting p50 and Bcl-2 during a viral infection. Here, we mechanistically demonstrated that UL41 can inhibit p50 expression and Bcl-2 (Fig. 6). Through mitochondrial isolation experiments, we found that UL41 is localized to the mitochondria and facilitates the release of Cyto-C from the mitochondria into cytoplasm. Our data strongly supports that UL41 can promote apoptosis via the mitochondrial-apoptotic pathway. In the subfamily of herpesviruses A, the highly conserved protein in the VHS polypeptide, EADD, is

considered to be the key RNase active site. To investigate whether PRV UL41 plays a key role in viral escape, we mutated conserved residues E192, D194, and D195 of PRV UL41. In our study, we demonstrated that PRV UL41-M successfully reverted to IRF3-induced levels of IFN-β expression and lost its ability to interact with IRF3 and its ability to suppress TNF-α-mediated pro-inflammatory cytokine activation (Fig. 7).

There are several limitations in this study. Experiments were performed under the condition of UL41 overexpression. Our study primarily aims to elucidate the biochemical mechanism by which UL41 antagonizes inflammatory pathway mediators. To conclusively demonstrate that UL41 is responsible for dampening antiviral responses during PRV infection, a PRV UL41-mutant strain should be used. However, we did show that siRNA-mediated knockdown of UL41 during a natural PRV infection restored PRV-mediated degradation of endogenous p-IRF3 and NF-kB, and inhibited IFN-β and IL-6 responses (Fig. 8). This indicates that the loss of UL41 restored antiviral responses during a PRV infection.

VHS, encoded by the *UL41* gene, participates in the assembly of viral particles during the late stages of viral infection. In fact, VHS from many α-herpesviruses contains conserved RNase-active residues (Liu et al., 2016). VHS is a member of the FEN-1 endonuclease family found in mammalian cells, yeast, and bacteria (Everly et al., 2002). It shares homologs with the neurotropic or α-subfamily of herpesviruses, such as HSV-1, HSV-2, and varicella-zoster virus. Conversely, VHS homologs are absent in the β-herpesviruses, represented by the cytomegaloviruses, or the γ-herpesviruses, such as Epstein–Barr virus (EBV) and Kaposi Sarcoma Herpesvirus (KSHV). The *UL41* gene has long been recognized as the virion host shutoff gene in numerousα-herpesviruses. Prior research has shown that HSV-1 can rapidly degrade pre-existing host mRNA, including β-actin, through the RNase activity of the VHS protein (Strom and Frenkel, 1987). The VHS protein is an IFN-I resistance factor with RNase activity. HSV-2 VHS protein has been shown to inhibit the production of antiviral factors through innate immune signaling pathways mediated by TLR2/3 and the RNA-sensing pathway, RIG-I/MDA5 (Khellaf et al., 2022). Infection of primary mouse embryonic blastocytes with a VHS-deficient strain of HSV-2 virus, restored HSV-2-induced viral infection, suggesting that VHS protein is critical in the viral infection process. Duck plague virus (DPV) UL41 has been shown to broadly inhibit RIG-I, MDA5, MAVS, STING, TBK1 and IRF7-mediated activation of IFN-β responses (He et al., 2022). BoHV-1 UL41 protein was also reported to inhibit the expression of ISGs by directly targeting STAT1 transcription, thereby antagonizing innate immune signaling pathways (Ma et al., 2019). This evidence allows us to study the impact of PRV VHS on the cGAS-STING signaling pathway and NF-κB signaling pathway. The involvement of PRV UL41 in key natural immune signaling pathways is intriguing. Subsequent research has revealed the critical role of PRV UL41 in these two signaling pathways.

5. Conclusions

Here, we biochemically and mechanistically show that the PRV late protein VHS, encoded by *UL41* gene, is a novel IFN antagonist. UL41 hinders the evasion strategy of antiviral factors by suppressing NF-κB and blocking the translocation of phosphorylated IRF3 into the nucleus. We further elucidate that the VHS protein exerts its ability to evade host antiviral responses through its RNase domain. These results will contribute to a better understanding of the mechanistic regulation of host antiviral inhibition by PRV UL41, and provide key information for the effective regulation of PRV pathogenesis.

Data availability

All the data generated during the current study are included in the manuscript. The raw data supporting the conclusions of this article will be made available by the authors, without undue reservation.

Ethics statement

This article does not contain any studies with human or animal subjects performed by any authors.

Author contributions

Zhenfang Yan: conceptualization, formal analysis, investigation, writing original draft, writing-review and editing. Jiayu Yue: data curation, methodology, writing-original draft. Yaxin Zhang: methodology, supervision. Zhengyang Hou: methodology, supervision. Dianyu Li: methodology. Yanmei Yang: methodology. Xiangrong Li: methodology. Adi Idris: writing-review and editing. Huixia Li: methodology. Shasha Li: methodology, supervision. Jingying Xie: conceptualization, funding acquisition, resources, supervision. Ruofei Feng: funding acquisition, resources, supervision, project administration. All authors have read and agreed to the published version of the manuscript.

Conflict of interest

All authors declare that there are no competing interests.

Acknowledgments

This work was supported by the Fundamental Research Funds for the Central Universities (31920230001), and Gansu Youth Science and Technology Fund Project (22JR5RA193 and 21JR1RA212).

Appendix A. Supplementary data

Supplementary data to this article can be found online at https://doi.org/10.1016/j.virs.2024.05.009.

References

Bardel, E., Doucet-Ladeveze, R., Mathieu, C., Harandi, A.M., Dubois, B., Kaiserlian, D., 2016. Intradermal immunisation using the TLR3-ligand poly (I:C) as adjuvant induces mucosal antibody responses and protects against genital HSV-2 infection. NPJ Vaccines 1, 16010.

Choi, Y., Bowman, J.W., Jung, J.U., 2018. Autophagy during viral infection - a double-edged sword. Nat. Rev. Microbiol. 16, 341–354.

Czerkies, M., Korwek, Z., Prus, W., Kochańczyk, M., Jaruszewicz-Błońska, J., Tudelska, K., Błoński, S., Kimmel, M., Brasier, A.R., Lipniacki, T., 2018. Cell fate in antiviral response arises in the crosstalk of IRF, NF-κb and JAK/STAT pathways. Nat. Commun. 9, 493.

Dauber, B., Poon, D., Dos Santos, T., Duguay, B.A., Mehta, N., Saffran, H.A., Smiley, J.R., 2016. The herpes simplex virus virion host shutoff protein enhances translation of viral true late mrnas independently of suppressing protein kinase R and stress granule formation. J. Virol. 90, 6049–6057.

Deng, L., Xu, Z., Li, F., Zhao, J., Jian, Z., Deng, H., Lai, S., Sun, X., Geng, Y., Zhu, L., 2022. Insights on the cGAS-STING signaling pathway during herpesvirus infections. Front. Immunol. 13, 931885.

Desloges, N., Rahaus, M., Wolff, M.H., 2005. The varicella-zoster virus-mediated delayed host shutoff: open reading frame 17 has no major function, whereas immediate-early 63 protein represses heterologous gene expression. Microb. Infect. 7, 1519–1529.

Drolet, M., Brisson, M., Schmader, K.E., Levin, M.J., Johnson, R., Oxman, M.N., Patrick, D., Blanchette, C., Mansi, J.A., 2010. The impact of herpes zoster and postherpetic neuralgia on health-related quality of life: a prospective study. CMAJ (Can. Med. Assoc. J.) 182, 1731–1736.

Ersing, I., Bernhardt, K., Gewurz, B.E., 2013. NF-κb and IRF7 pathway activation by Epstein-Barr virus latent membrane protein 1. Viruses 5, 1587–1606.

Everly Jr., D.N., Feng, P., Mian, I.S., Read, G.S., 2002. mRNA degradation by the virion host shutoff (VHS) protein of herpes simplex virus: genetic and biochemical evidence that VHS is a nuclease. J. Virol. 76, 8560–8571.

Ge, Z., Ding, S., 2022. Regulation of cGAS/STING signaling and corresponding immune escape strategies of viruses. Front. Cell. Infect. Microbiol. 12, 954581.

Geiss, B.J., Smith, T.J., Leib, D.A., Morrison, L.A., 2000. Disruption of virion host shutoff activity improves the immunogenicity and protective capacity of a replication-incompetent herpes simplex virus type 1 vaccine strain. J. Virol. 74, 11137–11144.

Ghosh, S., May, M.J., Kopp, E.B., 1998. NF-kappa B and Rel proteins: evolutionarily conserved mediators of immune responses. Annu. Rev. Immunol. 16, 225–260.

Han, Y., Xie, J., Xu, S., Bi, Y., Li, X., Zhang, H., Idris, A., Bai, J., Feng, R., 2021. Encephalomyocarditis virus abrogates the interferon beta signaling pathway via its structural protein VP2. J. Virol. 95, e01590-20.
He, T., Wang, M., Cheng, A., Yang, Q., Jia, R., Wu, Y., Huang, J., Tian, B., Liu, M., Chen, S., Zhao, X.X., Zhu, D., Zhang, S., Ou, X., Mao, S., Gao, Q., Sun, D., 2021. DPV UL41 gene encoding protein induces host shutoff activity and affects viral replication. Vet. Microbiol. 255, 108979.
He, T., Wang, M., Cheng, A., Yang, Q., Wu, Y., Jia, R., Chen, S., Zhu, D., Liu, M., Zhao, X., Zhang, S., Huang, J., Tian, B., Ou, X., Mao, S., Sun, D., Gao, Q., Yu, Y., Zhang, L., Liu, Y., 2022. Duck plague virus UL41 protein inhibits RIG-I/MDA5-mediated duck IFN-β production via mRNA degradation activity. Vet. Res. 53, 22.
He, T., Wang, M., Cheng, A., Yang, Q., Wu, Y., Jia, R., Liu, M., Zhu, D., Chen, S., Zhang, S., Zhao, X.X., Huang, J., Sun, D., Mao, S., Ou, X., Wang, Y., Xu, Z., Chen, Z., Zhu, L., Luo, Q., Liu, Y., Yu, Y., Zhang, L., Tian, B., Pan, L., Rehman, M.U., Chen, X., 2020. Host shutoff activity of VHS and SOX-like proteins: role in viral survival and immune evasion. Virol. J. 17, 68.
Hour, T.C., Chen, L., Lin, J.K., 2000. Suppression of transcription factor NF-kappaB activity by Bcl-2 protein in NIH3T3 cells: implication of a novel NF-kappaB p50-Bcl-2 complex for the anti-apoptotic function of Bcl-2. Eur. J. Cell Biol. 79, 121–129.
Jiang, F.F., Wang, R.Q., Guo, C.Y., Zheng, K., Liu, H.L., Su, L., Xie, S.S., Chen, H.C., Liu, Z.F., 2022. Phospho-proteomics identifies a critical role of ATF2 in pseudorabies virus replication. Virol. Sin. 37, 591–600.
Jin, X., Wang, W., Zhao, X., Jiang, W., Shao, Q., Chen, Z., Huang, C., 2023. The battle between the innate immune cGAS-STING signaling pathway and human herpesvirus infection. Front. Immunol. 14, 1235590.
Karin, M., Cao, Y., Greten, F.R., Li, Z.W., 2002. NF-kappaB in cancer: from innocent bystander to major culprit. Nat. Rev. Cancer 2, 301–310.
Khellaf, L., Bouscarat, F., Burrel, S., Fidouh, N., Hachon, L., Bucau, M., Lariven, S., Boutolleau, D., Joly, V., Ghosn, J., Le Pluart, D., Thy, M., 2022. Novel mutations in antiviral multiresistant HSV-2 genital lesion: a case report. J. Med. Virol. 94, 6122–6126.
Liu, Y.F., Tsai, P.Y., Chulakasian, S., Lin, F.Y., Hsu, W.L., 2016. The pseudorabies virus VHS protein cleaves RNA containing an IRES sequence. FEBS J. 283, 899–911.
Liu, Y.F., Tsai, P.Y., Lin, F.Y., Lin, K.H., Chang, T.J., Lin, H.W., Chulakasian, S., Hsu, W.L., 2015. Roles of nucleic acid substrates and cofactors in the VHS protein activity of pseudorabies virus. Vet. Res. 46, 141.
Ma, W., Wang, H., He, H., 2019. Bovine herpesvirus 1 tegument protein UL41 suppresses antiviral innate immune response via directly targeting STAT1. Vet. Microbiol. 239, 108494.
Ma, Z., Bai, J., Jiang, C., Zhu, H., Liu, D., Pan, M., Wang, X., Pi, J., Jiang, P., Liu, X., 2023. Tegument protein UL21 of alpha-herpesvirus inhibits the innate immunity by triggering cGAS degradation through TOLLIP-mediated selective autophagy. Autophagy 19, 1512–1532.
Meier, R.K., Ruiz-Fons, F., Ryser-Degiorgis, M.P., 2015. A picture of trends in Aujeszky's disease virus exposure in wild boar in the Swiss and European contexts. BMC Vet. Res. 11, 277.
Ming, S.L., Zhang, S., Wang, Q., Zeng, L., Zhou, L.Y., Wang, M.D., Ma, Y.X., Han, L.Q., Zhong, K., Zhu, H.S., Bai, Y.L., Yang, G.Y., Wang, J., Chu, B.B., 2022. Inhibition of USP14 influences alphaherpesvirus proliferation by degrading viral VP16 protein via ER stress-triggered selective autophagy. Autophagy 18, 1801–1821.
Nomura, M., Shimizu, S., Ito, T., Narita, M., Matsuda, H., Tsujimoto, Y., 1999. Apoptotic cytosol facilitates bax translocation to mitochondria that involves cytosolic factor regulated by bcl-2. Cancer Res. 59, 5542–5548.
Novak, I., Kirkin, V., McEwan, D.G., Zhang, J., Wild, P., Rozenknop, A., Rogov, V., Löhr, F., Popovic, D., Occhipinti, A., Reichert, A.S., Terzic, J., Dötsch, V., Ney, P.A., Dikic, I., 2010. Nix is a selective autophagy receptor for mitochondrial clearance. EMBO Rep. 11, 45–51.
Page, H.G., Read, G.S., 2010. The virion host shutoff endonuclease (UL41) of herpes simplex virus interacts with the cellular cap-binding complex eIF4F. J. Virol. 84, 6886–6890.
Pasieka, T.J., Lu, B., Crosby, S.D., Wylie, K.M., Morrison, L.A., Alexander, D.E., Menachery, V.D., Leib, D.A., 2008. Herpes simplex virus virion host shutoff attenuates establishment of the antiviral state. J. Virol. 82, 5527–5535.
Perkins, N.D., 2007. Integrating cell-signalling pathways with NF-kappaB and IKK function. Nat. Rev. Mol. Cell Biol. 8, 49–62.
Pheasant, K., Möller-Levet, C.S., Jones, J., Depledge, D., Breuer, J., Elliott, G., 2018. Nuclear-cytoplasmic compartmentalization of the herpes simplex virus 1 infected cell transcriptome is co-ordinated by the viral endoribonuclease vhs and cofactors to facilitate the translation of late proteins. PLoS Pathog. 14, e1007331.
Pomeranz, L.E., Reynolds, A.E., Hengartner, C.J., 2005. Molecular biology of pseudorabies virus: impact on neurovirology and veterinary medicine. Microbiol. Mol. Biol. Rev. 69, 462–500.
Popli, S., Chakravarty, S., Fan, S., Glanz, A., Aras, S., Nagy, L.E., Sen, G.C., Chakravarti, R., Chattopadhyay, S., 2022. IRF3 inhibits nuclear translocation of NF-κB to prevent viral inflammation. Proc. Natl. Acad. Sci. U.S.A. 119, e2121385119.
Radtke, K., Kieneke, D., Wolfstein, A., Michael, K., Steffen, W., Scholz, T., Karger, A., Sodeik, B., 2010. Plus- and minus-end directed microtubule motors bind simultaneously to herpes simplex virus capsids using different inner tegument structures. PLoS Pathog. 6, e1000991.
Samady, L., Costigliola, E., MacCormac, L., McGrath, Y., Cleverley, S., Lilley, C.E., Smith, J., Latchman, D.S., Chain, B., Coffin, R.S., 2003. Deletion of the virion host shutoff protein (vhs) from herpes simplex virus (HSV) relieves the viral block to dendritic cell activation: potential of vhs- HSV vectors for dendritic cell-mediated immunotherapy. J. Virol. 77, 3768–3776.
Sandbaumhüter, M., Döhner, K., Schipke, J., Binz, A., Pohlmann, A., Sodeik, B., Bauerfeind, R., 2013. Cytosolic herpes simplex virus capsids not only require binding inner tegument protein pUL36 but also pUL37 for active transport prior to secondary envelopment. Cell Microbiol. 15, 248–269.
Sehl, J., Teifke, J.P., 2020. Comparative pathology of pseudorabies in different naturally and experimentally infected species-A review. Pathogens 9, 633.
Stokol, T., Soboll, Hussey G., 2019. Editorial: current research in equid herpesvirus type-1 (EHV-1). Front. Vet. Sci. 6, 492.
Strom, T., Frenkel, N., 1987. Effects of herpes simplex virus on mRNA stability. J. Virol. 61, 2198–2207.
Sun, M., Hou, L., Tang, Y.D., Liu, Y., Wang, S., Wang, J., Shen, N., An, T., Tian, Z., Cai, X., 2017. Pseudorabies virus infection inhibits autophagy in permissive cells *in vitro*. Sci. Rep. 7, 39964.
Tan, L., Yao, J., Yang, Y., Luo, W., Yuan, X., Yang, L., Wang, A., 2021. Current status and challenge of pseudorabies virus infection in China. Virol. Sin. 36, 588–607.
Wang, D., Tao, X., Fei, M., Chen, J., Guo, W., Li, P., Wang, J., 2020. Human encephalitis caused by pseudorabies virus infection: a case report. J. Neurovirol. 26, 442–448.
Wang, G., Zha, Z., Huang, P., Sun, H., Huang, Y., He, M., Chen, T., Lin, L., Chen, Z., Kong, Z., Que, Y., Li, T., Gu, Y., Yu, H., Zhang, J., Zheng, Q., Chen, Y., Li, S., Xia, N., 2022. Structures of pseudorabies virus capsids. Nat. Commun. 13, 1533.
Wu, Y., Jin, S., Liu, Q., Zhang, Y., Ma, L., Zhao, Z., Yang, S., Li, Y.P., Cui, J., 2021. Selective autophagy controls the stability of transcription factor IRF3 to balance type I interferon production and immune suppression. Autophagy 17, 1379–1392.
Xie, W., Tian, S., Yang, J., Cai, S., Jin, S., Zhou, T., Wu, Y., Chen, Z., Ji, Y., Cui, J., 2022. OTUD7B deubiquitinates SQSTM1/p62 and promotes IRF3 degradation to regulate antiviral immunity. Autophagy 18, 2288–2302.
Ye, R., Su, C., Xu, H., Zheng, C., 2017. Herpes simplex virus 1 ubiquitin-specific protease UL36 abrogates NF-κB activation in DNA sensing signal pathway. J. Virol. 91, e02417-16.
Zhang, P., Su, C., Jiang, Z., Zheng, C., 2017. Herpes simplex virus 1 UL41 protein suppresses the IRE1/XBP1 signal pathway of the unfolded protein response via its RNase activity. J. Virol. 91, e02056-16.